Optics Letters

User-specific power level allocation optimization for OFDM-NOMA in a multi-user RoF system

Jin Shi,[1,2] You-Wei Chen,[2] Jing He,[1,*] Zhihua Zhou,[1] Xinda Yan,[1] Run-Kai Shiu,[2] and Gee-Kung Chang[2]

[1]College of Computer Science and Electronic Engineering, Hunan University, Changsha 410082, China
[2]School of Electrical and Computer Engineering, Georgia Institute of Technology, Atlanta, Georgia 30308, USA
*Corresponding author: jhe@hnu.edu.cn

Received 5 June 2020; accepted 29 June 2020; posted 2 July 2020 (Doc. ID 399586); published 6 August 2020

In this Letter, we propose a digital signal processing (DSP) -aided technique to optimize the power ratio among users for orthogonal frequency division multiplexing (OFDM) -based non-orthogonal multiple access (NOMA) in an integrated optical fiber and millimeter wave (mmWave) wireless communication system. In this way, a central or distributed unit can leverage the proposed techniques to maintain the uniformity of the signal-to-noise ratios (SNRs) among subcarriers without requiring any channel information feedback. The proposed mechanism can facilitate the power allocation management by treating all subcarriers equally as an independent channel. As an illustration, multiple NOMA scenarios, in which a near user with 10 km fiber transmission and far user with either longer fiber distance or additional wireless propagation, are experimentally investigated. Experimental results demonstrate that when the conventional OFDM-NOMA without the proposed DSP-aided technique is used, the optimal power ratios vary rapidly when the subcarrier quality index changes due to high-frequency fading in a mmWave radio over fiber (RoF) system, whereas, by using the proposed techniques, including both orthogonal circulant matrix transform and discrete Fourier transform, the optimal power ratios on all effective subcarriers are optimized at the same level and the users' performance is significantly improved.

https://doi.org/10.1364/OL.399586

For fifth-generation mobile communication and beyond, new radio access network (RAN) architecture has been proposed [1,2], where central unit (CU), distributed unit (DU), and remote unit (RU) are employed for providing flexible interface functionalities. The ever-increasing demand of wireless data services has prompted the mobile fronthaul (MFH), connecting DU and RU by using fiber links, toward larger capacity and lower latency [3,4]. Several solutions have been proposed to address the challenges compelled by next-generation communication network. Digitized common public radio interface (CPRI), as a standard interface protocol, combining with digital radio over fiber (RoF) is an existing solution and commercially used in 4G by major vendors. However, it is facing major challenges to reach higher capacity in 5G and beyond. Hence, the analog RoF (ARoF) system, integrating both the optical access network and wireless service, has been widely discussed in the literature and standardization forums to mitigate the aforementioned issues [5,6]. In ARoF, high-order and high spectral efficiency signals can be converted into analog signals by a digital-to-analog converter (DAC). Next, the optical modulated signals with analog waveforms are sent to RU through the optical access network infrastructure. In RU, the optical signal is directly converted back into an electrical radio frequency (RF) signal for wireless transmission.

In order to boost the data rate in wireless communication, higher frequency bands such as Q-, V-, and W-bands of millimeter waves (mmWave) becomes an important resource to employ due to its abundant raw bandwidth. Since the high-frequency mmWave beam is directional and suffering high propagation losses, line-of-sight and beamforming transmission are required. Driven by massive user access requirements due to the Internet of things (IoTs) and device to device communication in 5G and beyond, dense RUs are required to deploy for ubiquitous mobile access. Moreover, one RU is expected to simultaneously provide access to more users with advanced multiple access techniques [7].

Non-orthogonal multiple access (NOMA) has been widely investigated since it provides higher capacity and connects more users compared to orthogonal frequency-division multiplexing (OFDM) due to its additional dimension multiplexing, e.g., power domain [7–13]. In a NOMA-based system, multiple users with diverse channel conditions can share the same time and frequency resource block. Allocation of power ratio among users can greatly impact users' performance. Regarding the power allocation strategy, users with high signal-to-noise ratio (SNRs) are normally allocated with small power weights and vice versa. By combining NOMA with multi-carrier signals, e.g., OFDM, it can maximize the spectral efficiency and inherit some advantages such as resistance to inter-carrier interference (ICI) and inter-symbol interference (ISI). OFDM-NOMA has been investigated in a variety of research areas including the mmWave RoF system and optical wireless system.

In mmWave RoF systems, the users served by the same RU are experiencing different channel conditions as the mmWave

is susceptible to an obstacle, antenna misalignment, as well as device orientation. These factors will cause different SNRs on subcarriers, which imply that optimal power ratios on subcarriers may be adjustable in an OFDM-NOMA scenario. In prior literature [7–13], the power ratio is always optimized on a user-based granularity without considering the SNR difference among subcarriers, resulting in a sub-optimal performance. As such, to achieve globally optimal performance in OFDM-NOMA, power ratios on each subcarrier are essential to calibrate according to the availability of channel state information, which induces much complexity and relatively latency. Most importantly, it is barely feasible for practical implementation.

In this paper, a channel independent DSP-aided technique is proposed for OFDM-NOMA in a 57 GHz mmWave RoF system. It can transform uneven SNR distribution into a flat and stable profile across subcarriers without any channel feedback. Therefore, optimal power allocation independent of subcarrier quality index can be achieved. Both orthogonal circulant matrix transform (OCT) and discrete Fourier transform (DFT) -based schemes are experimentally demonstrated. When adopting OCT or DFT techniques, optimal power ratios remain consistent on different subcarriers. Furthermore, OFDM-NOMA with the proposed coding technique exhibits significant performance improvement after a 10 km standard single mode fiber (SSMF) and 1 m wireless transmission.

Assuming two users, i.e., UE1 and UE2, are taken into account, the messages transmitted by both users are denoted as S_1 and S_2, and OFDM is used for each user. Before signal overlapping, the corresponding power factors are set to α_1 and α_2, respectively, under a fixed total power. Therefore, the resulting NOMA signal is denoted as $\sum_{i=1}^{2}\sqrt{\alpha_i}s_i$. After channel propagation, the received signal can be represented as

$$y_i = h_i \sum_{i=1}^{2} \sqrt{\alpha_1} s_i + w_i, \tag{1}$$

where h_i is the transmission channel from DU to target UE$_i$. w_i is the additive white Gaussian noise (AWGN) of user i with zero mean and variance δ_n. Suppose UE2 is closer to RU than UE1, i.e., UE2 has higher channel gain. Therefore, UE2 is allocated with less power due to its good channel condition. Under the constraint of the total power, UE1 is, hence, allocated with more power, owing to its poor channel condition. To decode UE1, it is directly decoded by treating UE2 as noise, whereas, unlike UE1, UE2 needs to remove the interference caused by UE1. Thus, the successive interference cancellation (SIC) algorithm is used, i.e., the received signal is first decoded to recover UE1, which has large power allocation, then subtracts it to obtain UE2. The maximum data rates for UE1 and UE2 are shown as follows [14]:

$$\begin{aligned} R_1 &= \log_2(1+\alpha_1|h_1|^2/\delta_n), \\ R_2 &= \log_2\left(1+\frac{\alpha_2|h_2|^2}{\alpha_1|h_2|^2+\delta_n}\right). \end{aligned} \tag{2}$$

It can be seen that the achievable data rate is directly related to the power ratio. In most NOMA scenarios, power ratio is simply based on the user without considering the optimization on each subchannel in multi-carrier modulation-based NOMA systems. Nevertheless, in the frequency fading channel, the power ratio may vary in different channels. Hence, in order to maximum the throughput on each subchannel, an optimal power ratio on each subchannel is necessary. To avoid the power ratio update of every subchannel, two channel independent DSP-aided techniques including OCT and DFT techniques are proposed in OFDM-NOMA to solve the issue. Assuming every OFDM-NOMA symbol occupies N effective subcarriers, the OCT precoding matrix with $N \times N$ dimension is denoted as $C_{\mathrm{OCT}} = \{c_1, c_2, \ldots C_N; c_N, c_1, \ldots c_{N-1}; c_2, c_3, \ldots c_1\}$, where c_i is the corresponding Zadoff–Chu sequence [15,16]. The DFT coding matrix can be written as $C_{\mathrm{DFT}} = \{w^0, w^0 \ldots w^0; w^0, w^1 \ldots w^{N-1}; w^0, w^{N-1}, \ldots w^{(N-1)2}\}$, where $w = e^{-2\pi/N}$ [17,18]. By multiplying with mapped complex signal $\boldsymbol{S}$, the coding signal can be denoted as $\boldsymbol{Z} = \boldsymbol{C} \times \boldsymbol{S}$. At the receiver, the received equalized signal is multiplied by the corresponding inverse matrix to recover user information. By equalizing all subchannels using either the OCT or DFT technique, all subchannels will have a uniform channel gain. Hence, the channel state information of each subchannel is no longer needed, and the optimal power ratios on all subchannels can be united by one value, leading to power allocation being simple yet optimal. It is worth noting that by using direct computation, they both have the same computational complexity of $O(N^2)$. Whereas, since fast Fourier transform (FFT) can be used to compute one cycle of the DFT, its computational complexity can be reduced to $O(N * \log N)$. Therefore, DFT precoding involves fewer calculation resources, as opposed to OCT precoding.

Figure 1 shows the experimental setup of the DSP-assisted OFDM-NOMA-based 57 GHz mmWave RoF system. In order to overlap two OFDM signals in the power domain, two independent data streams serving UE1 and UE2 are generated by two pseudo-random binary sequence generators (PRBS). Then, every two binary bits are mapped into quadrature phase shift keying (QPSK) complex symbols. The complex symbols are scaled according to the power weights. The scaled QPSK symbols are directly overlapped in the power domain to generate power domain NOMA. Subsequently, optional coding techniques are performed. To generate real-valued signals for intensity modulation, Hermitian symmetry is imposed in the other half of the subcarriers before inverse FFT (IFFT) processing, which has a block size of 1024, 353 of which are modulated with effective data. Then, a CP with a 64-point sample is appended to the beginning of every OFDM-NOMA symbol to avoid ISI. Two training symbols (TSs) aiming for symbol synchronization and channel estimation are inserted at the beginning of every OFDM-NOMA frame. After parallel to serial (P/S) conversion, the generated OFDM-NOMA signal with an oversampling factor of 4 is fed into a DAC at a baud rate of 16 GS/s. Thus, it can be concluded that the OFDM signal has a bandwidth of 0.69 GHz, and each user can achieve a data rate of 2.6 Gb/s ($\frac{16\,\mathrm{GS/s}}{4} \times \frac{353}{1024+64} \times 2\,\mathrm{bit/symbol} \approx 2.6\,\mathrm{Gb/s}$). Since two users are overlapped in the power domain, the aggregate data rate is 5.2 Gb/s. The electrical signal is then used to drive a directly modulated laser (DML) for electrical-to-optical conversion. After 10/20 km SSMF transmission, an attenuator (ATT) is placed in front of the photodiode (PD) to adjust the received optical power (ROP). A sinewave signal with 14.298 GHz is generated by a local oscillator and then multiplied by four to generate a 57.2 GHz high-frequency sinewave. The mmWave signal is obtained by combining the electrical signal and 57.2 GHz RF signal in a mixer. Subsequently, the resulting 57.2 GHz mmWave electrical signal is transmitted

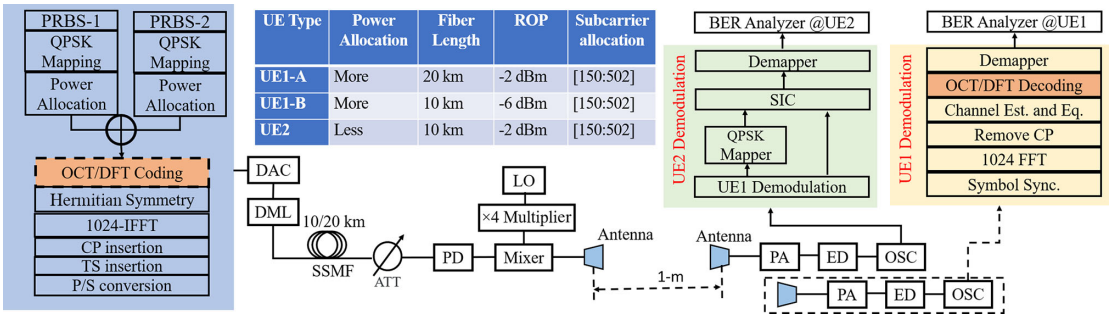

Fig. 1. Illustration of OFDM-NOMA-based mmWave RoF system using the OCT/DFT technique. Inset is the user configuration.

via 1 m free space transmission by a 25 dBi gain horn antenna. The mmWave signal is received by another horn antenna. An envelope detector is used for down-conversion from RF to intermediate frequency (IF) after the power amplifier (PA). Finally, the IF signal is sampled by a real-time oscilloscope for further offline processing. In our experiments, UE2 is playing a role of a good user and is fixed with 10 km SSMF transmission at the ROP of −2 dBm. On the contrary, we consider two different scenarios for UE1. One, referred to as UE1-A, is with a 20 km SSMF and at same ROP with regard to UE2. The fiber loss is about 0.18 dB/km. The other, termed as UE1-B, is at the ROP of −6 dBm but with the same fiber length with respect to UE2. The detailed user configuration is inserted in Fig. 1. It is worth noting that since mmWave wireless transmission is very sensitive to the position and angle of the pair of antennas, the position and angle are fixed in our experiments, and the ROP is adjusted instead to emulate the near user and far user.

At the receiver of UE1 with inferior channel condition, the detailed DSP blocks, is illustrated in Fig. 1. It is worth noting that the UE2 with less power allocation is directly treated as noise when decoding UE1. On the contrary, as for the demodulation of UE2, UE1 demodulation is first carried out and then re-mapped into QPSK symbols for SIC processing. After that, UE2 is decoded, and its bit error rate (BER) is calculated.

We first measure the channel SNR over subcarriers for three different scenarios without coding, with OCT and DFT, respectively, since the channel conditions in optical communication systems may be influenced by several specific parameters such as fiber length and loss, which will directly lead to the loss of signal power and thus can be reflected by channel SNR. It can be seen that UE2 has the best channel condition. The other two cases have farther distance either in fiber or wireless distance than UE2, and thus they are treated as poor users, i.e., UE1, which requires high-power allocation. It can be seen from Fig. 2 that, without the coding technique, the mmWave RoF system exhibits severe high-frequency fading, which is limited by some electrical devices like the envelope detector. Therefore, applying a uniform power ratio on all subcarriers is hardly optimal in such a frequency fading system. Enabled by the coding technique, both OCT and DFT techniques can make SNR curves flat, while it can be found that the DFT technique has a little higher SNR gain than OCT due to its peak to average power ratio (PAPR) reduction.

Figure 3 illustrates the optimal power ratio distribution on some high-frequency subcarriers for UE2. It can be seen that without the coding technique, the optimal power ratios dramatically vary on different subcarriers. However, by using

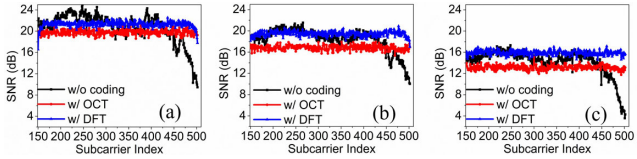

Fig. 2. Measured SNR versus subcarrier index for (a) UE2, (b) UE1-A, and (c) UE1-B.

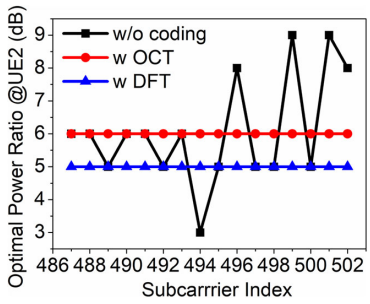

Fig. 3. Optimal power ratio distribution for UE2 on different subcarriers without coding with OCT and DFT techniques, respectively.

the coding technique, all subcarriers present nearly the same optimal power ratio thanks to the uniform SNR distribution. Therefore, aided by the channel independent coding techniques, user-specific power allocation is feasible while guaranteeing optimal performance on each subcarrier, which significantly reduces the processing delay. It is worth noting that though two-user-based NOMA is taken into account for the demonstration, the coding techniques are still applicable for NOMA with more than two users.

Afterwards, the BER performance without coding, with the OCT and DFT techniques, is further investigated. Figure 4(a) depicts the BER performance versus power ratio ($\alpha 1/\alpha 2$) for UE2. It can be seen that when the power ratio increases from the optimized point, i.e., less power is allocated to UE2, the BER performance of UE2 degrades. It is because that less power means lower SNR, while, when decreasing the power ratio, the BER performance deteriorates. It is attributed to the error propagation from the SIC process as UE1 with less power will cause an error propagation to UE2. The minimum BERs for UE2 without coding, with OCT and with DFT, are 1.4×10^{-3}, 9.0×10^{-5}, and 4.5×10^{-5}, respectively, which corresponds to the power ratios of 7 dB, 6 dB, and 5 dB, respectively. One can note that without OCT and DFT coding it is

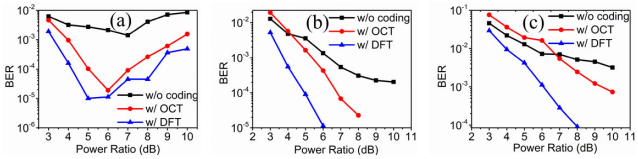

Fig. 4. BER performance versus power ratio for (a) UE2, (b) UE1-A, and (c) UE1-B.

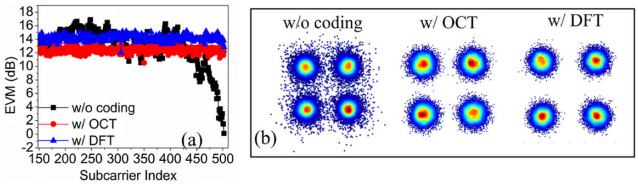

Fig. 5. (a) EVM versus subcarrier index for UE2 without coding, with OCT and DFT. (b) The corresponding constellations.

unlikely to obtain an optimized power setting with significant performance gain. Figures 4(b) and 4(c) illustrate the BER performance versus power ratio for the cases of UE1-A and UE1-B, respectively. It can be found that the BER performance of UE1 gradually improves with the increase of power ratio due to the enhancement of SNR. Meanwhile, UE1s with OCT and DFT generally exhibit better performance than that without the coding technique. UE1s with the DFT technique achieve better BER performance at any power ratio than that with the OCT technique due to its PAPR reduction as mentioned before. It is worth noting that when the channel condition is very poor, like very small ROP and very low power ratio, UE1s with the OCT technique will present poorer performance than that without the coding technique. It is because the compensation on non-uniform frequency response may result in the failure of all subcarriers to reach a certain decision threshold for QPSK while the average SNR is low.

According to Fig. 4(a), the optimal power ratios, which means minimum overall BER can be obtained, for UE2 without coding, with OCT and DFT are 7 dB, 6 dB, and 5 dB respectively. By fixing power ratios as that, Fig. 5(a) depicts the error vector magnitude (EVM) performance versus subcarrier index. Since the demodulation of UE2 needs an extra SIC process to eliminate interference, the overall EVM performance is remarkably below the measured SNR in Fig. 2(a) owing to error propagation. The EVM performance of UE2 without coding has a dramatic dropping on high-frequency subcarriers. However, the OCT and DFT techniques still exhibit uniform EVM on effective subcarriers for UE2. Figure 5(b) illustrates the corresponding constellations by using different techniques. It is evident that the constellations of UE2 employing a novel coding technique are clearer for threshold decisions than that without coding.

In conclusion, user-specific power allocation for OFDM-NOMA is investigated in an integrated fiber mmWave RoF system. Enabled by channel independent techniques, the requirement of estimating power ratios on different subcarriers is fully relaxed, such that system complexity is greatly reduced. Moreover, all subcarriers can be represented by the same power ratio while maintaining optimal performance. Multiple scenarios for NOMA users with different fiber or wireless distances are systematically demonstrated. Experimental results show that user-specific power level allocation optimization, which is independent of the subcarrier quality index, can be easily realized with the proposed coding techniques even under the power fading channel, and the users with OCT and DFT generally outperform that without coding techniques when varying the power ratio.

Funding. National Natural Science Foundation of China (61775054); China Scholarship Council (201906130124); Science and Technology Project of Hunan Province (2016GK2011).

Disclosures. The authors declare no conflicts of interest.

REFERENCES

1. I. Chih-Lin, H. Li, J. Korhonen, J. Huang, and L. Han, J. Lightwave Technol. **36**, 541 (2018).
2. G.-K. Chang and P.-C. Peng, in *23rd Opto-Electronics and Communications Conference (OECC)* (2018).
3. G.-K. Chang and L. Cheng, in *21st OptoElectronics and Communications Conference (OECC)* (2016), pp. 1–3.
4. F. Lu, M. Xu, S. Shen, Y. M. Alfadhli, H. J. Cho, and G.-K. Chang, in *Optical Fiber Communications Conference and Exposition (OFC)* (2018), paper M3K.4.
5. S. Liu, Y. M. Alfadhli, S. Shen, H. Tian, and G.-K. Chang, in *Optical Fiber Communications Conference and Exposition (OFC)* (2018), paper W4B.3.
6. "Transmission systems and media, digital systems and networks: radio over fibre systems," ITU-T G.9803 (2018).
7. F. Lu, M. Xu, L. Cheng, J. Wang, J. Zhang, and G.-K. Chang, J. Lightwave Technol. **34**, 4179 (2016).
8. F. Lu, M. Xu, L. Cheng, J. Wang, and G.-K. Chang, J. Lightwave Technol. **35**, 4145 (2017).
9. J. Shi, J. He, K. Wu, and J. Ma, J. Lightwave Technol. **37**, 5212 (2019).
10. B. Lin, W. Ye, X. Tang, and Z. Ghassemlooy, Opt. Express **25**, 4348 (2017).
11. X. Guan, Q. Yang, and C.-K. Chan, IEEE Photon. Technol. Lett. **29**, 377 (2017).
12. Y. Tian, K.-L. Lee, C. Lim, and A. Nirmalathas, in *Optical Fiber Communications Conference and Exposition (OFC)* (2018), paper Tu3J.4.
13. J. Shi, Y. Hong, R. Deng, J. He, L.-K. Chen, and G.-K. Chang, J. Lightwave Technol. **37**, 4401 (2019).
14. S. Marcano and H. L. Christiansen, IEEE Access **6**, 13587 (2018).
15. J. Ma, M. Chen, K. Wu, and J. He, J. Lightwave Technol. **37**, 6063 (2019).
16. Y. Hong and L.-K. Chen, in *18th International Conference on Transparent Optical Networks (ICTON)* (2016), pp. 1–4.
17. M. Chen, X. Xiao, Z. Huang, J. Yu, F. Li, Q. Chen, and L. Chen, J. Lightwave Technol. **34**, 2100 (2016).
18. M. Chen, L. Zhang, D. Xi, G. Liu, H. Zhou, and Q. Chen, IEEE Access **8**, 16838 (2020).